THE JOURNAL OF PHYSICAL CHEMISTRY C

Article

Cite This: J. Phys. Chem. C 2018, 122, 16639−16648

pubs.acs.org/JPCC

Modification of Optical Properties and Excited-State Dynamics by Linearizing Cyclic Paraphenylene Chromophores

B. Rodríguez-Hernández,[†] D. Ondarse-Álvarez,[†] N. Oldani,[†] A. Martínez-Mesa,[‡] Ll. Uranga-Piña,[‡] S. Tretiak,[§] and S. Fernández-Alberti*[,†]

[†]Universidad Nacional de Quilmes, Roque Saenz Peña 352, B1876BXD Bernal, Argentina

[‡]DynAMoS (Dynamical processes in Atomic and Molecular Systems), Facultad de Física, Universidad de La Habana, San Lázaro y L, La Habana 10400, Cuba

[§]Center for Nonlinear Studies (CNLS) and Center for Integrated Nanotechnologies (CINT), Los Alamos National Laboratory, Los Alamos, New Mexico 87545, United States

Supporting Information

ABSTRACT: Cyclic and bent conjugated molecular systems have tunable optical, structural, and dynamical features that differentiate them from their linear counterparts. Examples of such systems are [*n*]cycloparaphenylenes (CPPs), which consist of nanorings composed of *n* para-linked benzene units. Circular geometry and tunability of π-orbital overlaps and bending strains enrich them with unique physicochemical and electronic properties compared to those of the corresponding linear oligoparaphenylenes. Herein, we explore the changes of these properties on alkyl-tethered-*p*-heptaphenylenes by modifying the methylene tether lengths from 1 to 19 carbons, leading to a gradual linearization of the conjugated backbone conformation. For this purpose, the photoinduced internal conversion processes of different alkyl-tethered-*p*-heptaphenylenes are simulated using nonadiabatic excited-state molecular dynamics. We found that the greater the strain introduced on the conjugated system, the slower the electronic and vibrational energy relaxation process. All bent *p*-heptaphenylenes exhibit similar patterns of intramolecular energy redistribution that finally spatially localize the exciton on phenylene units in the middle of the conjugated chain. This behavior is opposite to the random exciton localization previously reported for [*n*]CPPs. Moreover, the nonadiabatic $S_2 \rightarrow S_1$ electronic transition activates specific collective asymmetric vibrational excitations that promote periodic oscillatory evolution of the excitonic wave function before an excessive energy dissipates into the bath degrees of freedom.

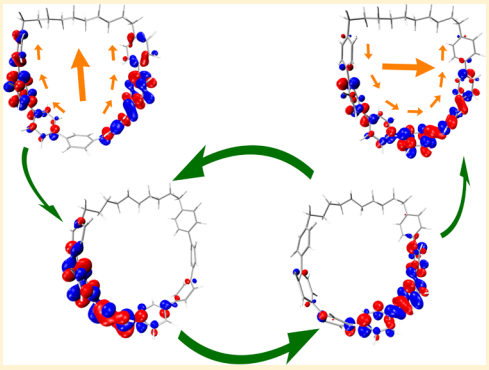

I. INTRODUCTION

Advances in organic synthesis lead to know π-conjugated organic polymeric materials with a large variety of well-defined tunable topologies that enhance their applications in the areas of molecular electronics and photovoltaics.[1−3] This introduces the challenge of establishing a connection between geometrical conformations and dynamics of energy transfer in the new molecular systems. Here, it is of particular interest to explore both experimentally and computationally the photoinduced electronic energy relaxation and redistribution prior to light emission. Following photoexcitation, distinct nonradiative relaxation pathways may trigger a number of complex processes that affect the desired functionalities such as emission efficiency. Internal conversion, intramolecular energy transfer, charge separation, and spatial localization of excitons (self-trapping) are examples of such processes.[4]

Cyclic conjugated molecular systems attracted interest of the scientific community[5] because of their unique physicochemical and electronic properties that make them suitable for potential applications in various technologies, such as light-emitting devices, nanoelectrodes, and mechanically controllable break junctions to name a few.[6] Among them, cycloparaphenylenes ([*n*]CPPs),[7−9] composed of *n* phenyl units linked at the para positions forming a conjugated periodic chain, raise an additional interest of being the smallest possible fragments of single-walled carbon nanotubes.[5,6,10−19] Larger [*n*]CPPs exhibit extremely high photoluminescence efficiencies.[20] Within their cyclic nanostructures, the efficiency of π-orbital overlaps competes with bending strains,[16,21] leading to an unusual ring-size dependence of their optoelectronic properties. On one hand, CPP linear optical absorption maximum wavelength results independent of their size (*n*), in contrast with its increase in linear [*n*]*p*-phenylenes ([*n*]LPPs).[6,9,14,15,22] On the other hand, [*n*]CCPs feature an increasing Stokes shift with a decrease of their size, being an opposite trend as to the one observed in their linear counterparts [*n*]LPPs.[17]

Received: June 11, 2018
Revised: July 9, 2018
Published: July 10, 2018

DOI: 10.1021/acs.jpcc.8b05582
J. Phys. Chem. C 2018, 122, 16639−16648

In an attempt to clarify the origin of size-dependent trends of the optoelectronic properties of [n]CCPs, Jasti et al.[23] have synthesized and characterized the optoelectronic properties of *m*-alkyl-tethered-*p*-heptaphenylenes with alkyl chains (*m*-alkyl-[7]PP) of various (m = 1−20) length. These experiments, performed on tetrahydrofuran as a solvent, have revealed that bending and cyclic conjugation provide novel materials with optoelectronic and solubility features that make them suitable as building blocks for synthesis of new conjugated organic materials. These systems span geometries in between circular and linear limiting cases (see Figure 1a). This experimental

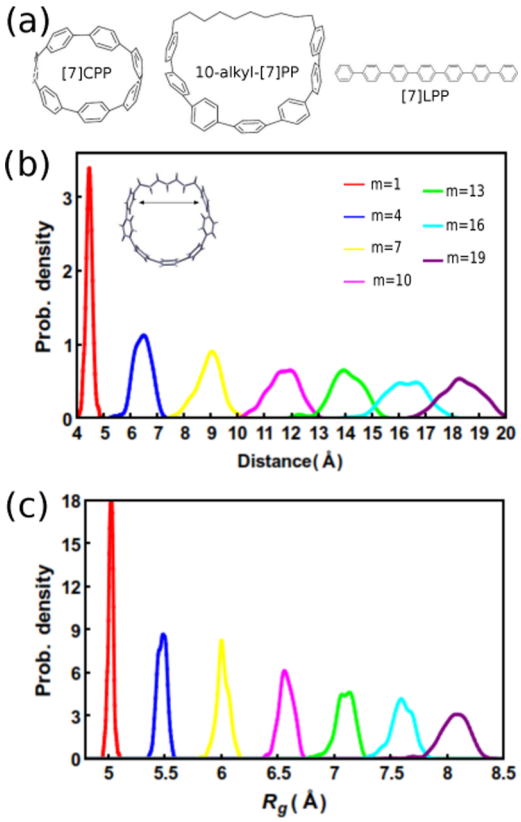

Figure 1. (a) Schematic representation of [7]CPP, 7-alkyl-[7]PP, and [7]LPP; density probability distributions (ρ) of (b) distances between phenyls at both ends of the phenylene moiety and (c) radius of gyrations for *m*-alkyl-[7]PPs (m = 1, 4, 7, 10, 13, 16, and 19) obtained from equilibrated ground-state molecular dynamics simulations at 300 K.

investigation reported that excitation to the lowest S_1 excited state becomes optically more allowed in *m*-alkyl-[7]PPs as the symmetry is broken by larger alkyl tethers. Additionally, the S_1 band (mainly composed of the highest occupied molecular orbital to lowest unoccupied molecular orbital transition) is getting systematically blue-shifted with the increasing m. Finally, this study also confirmed a slight increase of average torsional angles with an increasing m.

In this work, we extend the previous experimental work on *m*-alkyl-[7]PPs by performing systematic nonadiabatic excited-state molecular dynamics simulations. A Nonadiabatic EXcited-State Molecular Dynamics (NEXMD)[24,25] framework has been previously successfully applied to simulate the intramolecular electronic and vibrational energy relaxation and redistribution in many extended conjugated molecules.[24] Through NEXMD modeling, it was possible to achieve a detailed description of the internal conversion processes of [n]CPPs of different sizes.[22,26] In particular, we found that the excited state became more delocalized for smaller hoop sizes. This is a consequence of increased structural strain in smaller CPPs, which facilitates planarization of biphenyls. In addition, the efficient fluorescence in large [n]CPPs has been associated with the spatial localization of the exciton (self-trapping), which breaks the commonly used Condon approximation. In this article, we further explore these dynamic relationships among structural strains, electron−phonon couplings, exciton localization, and internal conversion rates for bent *p*-phenylenes tethered by alkyl chains. We analyze the dependence of photoinduced dynamics on the length of the alkyl chain, which ultimately controls the degree of bending of the paraphenylene moieties. As in the pioneering work of Jasti et al.,[23] we systematically relax the bending strain of bent *p*-phenylene units by inserting new $-CH_2-$ units to the alkyl tether. Therefore, an increase of the tether length is naively expected to mimic the size-dependent trends of the dynamical properties previously reported on [n]CPPs.[16,20−22,26] However, [n]CPPs have a fully conjugated structure and are lacking chain end-effects, whereas the alkyl tether breaks the conjugation in *m*-alkyl-[n]PPs. This significantly differentiates the exciton dynamics of these two classes of compounds.

The article is organized as follows. A brief overview of the NEXMD approach and relevant computational details are provided in Section II. Results and discussion are presented in Section III, and finally Section IV summarizes our main findings and concludes.

II. METHODS

II.I. NEXMD Background. The NEXMD[24,25,27] is an efficient method for the simulation of photoinduced dynamics of extended conjugated molecular systems involving manifold of coupled electronic excited states within the time scale of picoseconds. The NEXMD package achieves goal via direct nonadiabatic molecular dynamics modeling that combines the fewest switches surface hopping (FSSH) algorithm[28,29] with on the fly calculations of electronic excited-state energies $E_\alpha(\mathbf{R})$,[30−32] gradients $\nabla_R E_\alpha(\mathbf{R})$,[33,34] and nonadiabatic derivative couplings $\mathbf{d}_{\alpha\beta} = \langle \phi_\alpha(\mathbf{r};\mathbf{R})|\nabla_R \phi_\beta(\mathbf{r};\mathbf{R})\rangle$.[24,31,35,36] Here, $\mathbf{r}$ and $\mathbf{R}$ are the electronic and nuclear coordinates, respectively, and $\phi_\alpha(\mathbf{r};\mathbf{R})$ stands for the adiabatic excited states.

FSSH is a hybrid quantum/classical approach in which the nuclei evolve classically on a single adiabatic electronic excited state at any given time and hopping from one excited state to another can occur based on the nonadiabatic coupling strengths and a stochastic switching routine. Within the NEXMD framework, nuclei are propagated using the Langevin equation at constant temperature[25] as

$$M_i\ddot{\mathbf{R}}_i = -\nabla_R E_\alpha(\mathbf{R}) - \gamma M_i\dot{\mathbf{R}}_i + \mathbf{A}(t) \quad (1)$$

with M_i, $\ddot{\mathbf{R}}_i$, $\dot{\mathbf{R}}_i$, and $\mathbf{R}_i$ are the mass, acceleration, velocity, and position of the ith nuclei, respectively, and $\mathbf{A}(t)$ is the stochastic force that depends on the bath temperature, T, and the friction coefficient, γ (ps^{-1}).[37]

Meanwhile, the electronic wave function, $\psi(\mathbf{r},\mathbf{R})$, developed on the basis of adiabatic electronic states ($\psi(\mathbf{r},\mathbf{R},t) = \sum_\alpha c_\alpha(t)\phi_\alpha(\mathbf{r};\mathbf{R})$) is propagated using the time-dependent Schrödinger equation as

$$i\hbar\dot{c}_\alpha(t) = c_\alpha(t)E_\alpha(\mathbf{R}) - i\hbar\sum_\beta c_\beta(t)\dot{\mathbf{R}}\cdot\mathbf{d}_{\alpha\beta} \quad (2)$$

DOI: 10.1021/acs.jpcc.8b05582
J. Phys. Chem. C 2018, 122, 16639−16648

The collective electronic oscillator (CEO) approach[32,38,39] is used to calculate excited states at the configuration interaction single (CIS) level of theory with the semiempirical Austin model 1 Hamiltonian.[40] The CEO approach is based on the equation of motion[41] for the single-electron density matrix.[42] It has been successfully applied to a large variety of conjugated materials,[38,43−47] providing an adequate description of the manifold of coupled electronic excited states. Moreover, previous articles[22,26] have validated its use to simulate photoinduced dynamics in [*n*]CPPs. More details concerning the NEXMD implementation and parameters can be found elsewhere.[24,25,27] For example, to identify trivial unavoided crossings, we track the state identity using the min-cost algorithm.[48] In addition, the instantaneous decoherence approach[49] is introduced to account for electronic decoherence and to avoid numerical inconsistency in the FSSH algorithm.[28,29]

II.II. Transition Density (TD) Analysis. Within NEXMD simulations, changes in the spatial localization of the excited-state wave function can be tracked by following the evolution of the electronic transition density (TD) for the current state as a function of time. The CEO approach[38,39] calculates TD matrices whose elements can be written as

$$\rho_{nm}^{0\alpha}(t) = \langle \phi_\alpha(\mathbf{r};\, \mathbf{R}(t))|c_m^+ c_n|\phi_0(\mathbf{r};\, \mathbf{R}(t))\rangle \tag{3}$$

where $\phi_0(\mathbf{r};\, \mathbf{R}(t))$ and $\phi_\alpha(\mathbf{r};\, \mathbf{R}(t))$ represent the CIS adiabatic ground- and excited-state wave functions, respectively, n and m are the indices referring to the AO basis functions, and c_m^+ and c_n are the creation and annihilation operators. The diagonal elements $\rho_{nn}^{0\alpha}$ represent the changes in the distribution of electronic density caused by excitation from ground state S_0 to excited electronic state S_α.[50] for bound excitonic states with a minor charge transfer character[30,51] (Frenkel excitons) being the case of the present molecules.

The fraction of TD localized in specific fragments or units can be tracked during NEXMD simulations as

$$(\rho_X^{0\alpha}(t))^2 = \sum_{n_X m_X} (\rho_{n_X m_X}^{0\alpha}(t))^2 \tag{4}$$

where subindex X indicates atoms localized in the selected fragment of the molecule. In addition, the time-dependent (de)localization of the TD among several X fragments or units can be followed using the participation number (PN) given by

$$\mathrm{PN}(t) = [\sum_X ((\rho_X^{0\alpha}(t))^2)^2]^{-1} \tag{5}$$

Values of PN = 1 indicate the localization of the TD within a single fragment or unit, and PN = N corresponds to delocalization over the whole N fragments in which the molecule has been fragmented for analysis.

II.III. Computational Details. NEXMD simulations have been performed on [7]CPP, *m*-alkyl-[7]PPs (*m*-alkyl-[7]PPs (m = 1, 4, 7, 10, 13, 16, and 19), and linear 7-paraphenylene ([7]LPP) at room temperature (300 K) using the Langevin friction coefficient γ = 2.0 ps^{-1}. For each system, equilibrated ground-state molecular dynamics simulations of 7 ns were conducted using a time step of 0.5 fs. These simulations provide a good initial conformational sampling for NEXMD simulations. Five hundred snapshots, equispaced on time, were collected as initial geometries and momenta for the subsequent NEXMD simulations. Each of these initial configuration was instantaneously excited to an initial excited state α with frequency Ω_α and normalized oscillation strength f_α, selected according to a Gaussian-shaped Franck−Condon window defined as $g_\alpha(\mathbf{r}, \mathbf{R}) = f_\alpha \exp[-T^2[E_{\mathrm{laser}} - E_\alpha(\mathbf{R})]^2]$, E_{laser} being the energy of a laser pulse $f(t) = \exp(t^2/2T^2)$, centered at the maximum of the absorption for the S_2 state of a given molecule with T^2 = 42.5 fs corresponding to a full width at half-maximum of 100 fs.

For each system, 500 NEXMD simulations of 500 fs duration have been performed using a classical time step of 0.1 fs for nuclei propagation (eq 1) and a quantum time step of 0.025 fs to propagate the electronic coefficients (eq 2). Ten electronic excited states and their corresponding nonadiabatic couplings were included. To identify and deal with trivial unavoided crossings, we track the states using the min-cost algorithm as it has been described elsewhere.[48] In addition, an instantaneous decoherence approach, where electronic coefficients are reinitialized following attempted hop (either successful or forbidden), is introduced to account for electronic decoherence.[49] To identify and deal with trivial unavoided crossings, we track the states using the min-cost algorithm as it has been described elsewhere.[39] In addition, an instantaneous decoherence approach, where electronic coefficients are reinitialized following attempted hop (either successful or forbidden), is introduced to account for electronic decoherence.[49]

III. RESULTS AND DISCUSSION

Alkyl-tethered-*p*-phenylenes are molecular systems particularly suitable for a systematic analysis of the effect of bending strains on optical and dynamical properties, covering the range from linear ([*n*]LPP) to cyclic ([*n*]CPP) paraphenylenes (see Figure 1). NEXMD simulations briefly described in Section II have been performed on [7]CPP, *m*-alkyl-[7]PPs (m = 1, 4, 7, 10, 13, 16, and 19), and linear 7-paraphenylene ([7]LPP).

The ground state conformational sampling at T = 300 K explored on *m*-alkyl-[7]PPs (m = 1, 4, 7, 10, 13, 16 and 19) reveals that the degree of bending of the paraphenylene moieties can be effectively modulated by the tether length. Figure 1 shows distributions of distances between phenyls at both ends of the paraphenylene moiety (panel b) and radius of gyrations (R_g) for the different *m*-alkyl-[7]PPs (panel c). Both structural parameters gradually increase with an increasing tether length (m). Thus, for the molecular sequence considered, the distance between two terminal carbons in the conjugated chain increases from 1.4 Å (a single bond length in the perfect circle [7]CPP) and 4.5 Å (m = 1) to 18.5 Å (m = 19) and 23.0 Å (in a linear oligomer [7]LPP). Notably, the alkyl chain is moderately soft so that the width of geometry distribution increases from about 0.5 Å (m = 1) to 3 Å (m = 19). Such progressive extension of the alkyl tether systematically relaxes the bending strain of *p*-phenylenes units. Because of this reduction of steric hindrances, the average values of dihedral angles between the phenyl rings increase concomitantly with m (Figure 2).[52] This is consistent with the previous reported increase of the average values of dihedral angles with the size of [*n*]CPPs.[18,53,54] Nevertheless, whereas all [*n*]CPP dihedral angles present equivalent average values in the range of ≈30−40°,[26] this is not the case for *m*-alkyl-[7]PPs. The torsions involving the external phenylene units of the paraphenylene moiety, that is, those closer to the alkyl tether, seem to be independent of m with an average value at about 40°, ranging between values of ≈30 and 50° for m = 1 and [7]LPP, respectively (Figure 2a). Moreover, intermediate

DOI: 10.1021/acs.jpcc.8b05582
J. Phys. Chem. C 2018, 122, 16639−16648

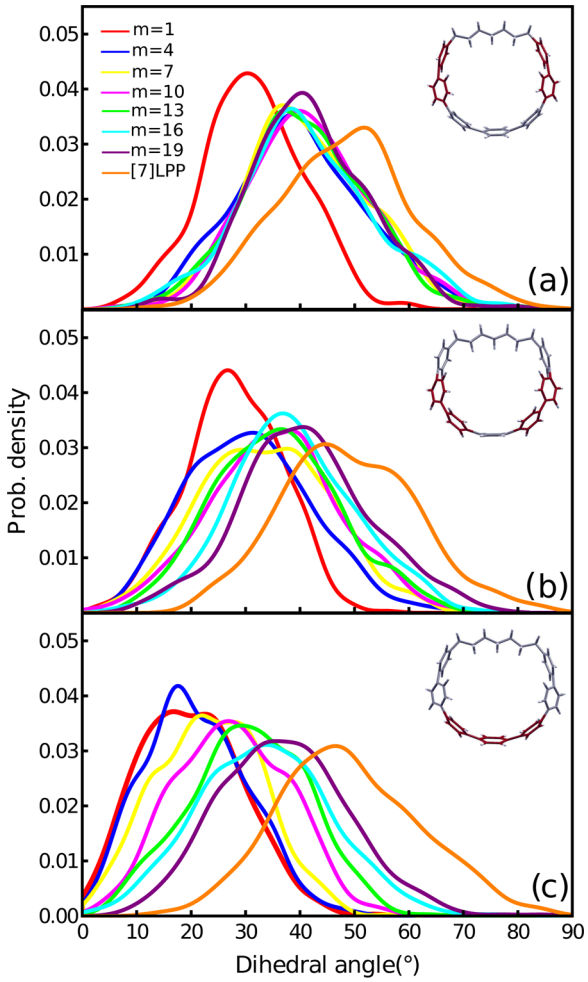

Figure 2. Dihedral angle distributions at the initial equilibrated ground-state configurations at 300 K for *m*-alkyl-[7]PPs (*m* = 1, 4, 7, 10, 13, 16, and 19) and [7]LPP. The corresponding neighboring phenyl rings involved in each dihedral angle are indicated in red in the schematic representation of the molecules.

torsions in Figure 2b show a minor dependence on *m*. In contrast, Figure 2c reveals a significant dependence on the tether length for the inner torsions. Therefore, the bending strains are not uniformly distributed on *m*-alkyl-[7]PPs. This points to a significant structural difference from [*n*]CPPs.

Figure 3 shows calculated absorption spectra at 300 K for [7]CPP, *m*-alkyl-[7]PPs (*m* = 1, 4, 7, 10, 13, 16, and 19), and [7]LPP. These are obtained as superposition of spectra from 500 individual conformers taken from the ground-state sampling and thus directly reflect observed torsional broadening (Figure 2) caused by thermal fluctuations. Overall, barring constant red shift by about 70 nm, the theoretical spectra agree well with their experimental counterparts.[23] We notice that S_1, S_2, and S_3 states show a blue shift with lengthening of the alkyl tether. These blue shifts are a consequence of the increase of the torsions between phenyl units (Figure 2) and disruption of conjugation. Moreover, the $S_0 \rightarrow S_1$ transition, optically forbidden in circular CPPs geometries due to symmetry, gradually becomes optically allowed, as symmetry is broken while increasing the length of the alkyl tether. Concomitantly, the $S_0 \rightarrow S_2$ transition appears for all *m* and $S_0 \rightarrow S_3$ transition becomes forbidden with the increasing *m*. These trends can be rationalized by analyzing Figure 4, where S_1, S_2, and S_3 state transition densities are plotted for several *m*-alkyl-[7]PPs, [7]CPPs, and [7]LPPs (S_4 state transition densities are also provided in Figure S1). The transition density of the α state represents changes in the distribution of electronic density caused by $S_0 \rightarrow S_\alpha$ photoexcitation. Therefore, it defines the transition dipole moment and thus the oscillator strength. As we can see, S_1, S_2, and S_3 wave functions carry 0, 1, and 2 nodes on the paraphenylene moieties of *m*-alkyl-[7]PPs, respectively. Bent geometries ensure constructive and destructive superpositions of individual transition dipole moments of phenylene units for S_2 and S_3 states, respectively. Nevertheless, these three states became optically allowed, showing equivalent oscillator strengths, due to structural distortions that break symmetry during the photoinduced excited-state dynamics (see Supporting Information (Figure S2)).

Using the NEXMD, we further simulate nonradiative electronic and vibrational energy relaxation and redistribution after initial photoexcitation in [7]CPP, *m*-alkyl-[7]PPs (*m* = 1, 4, 7, 10, 13, 16, and 19), and [7]LPP. Figure 5 shows calculated evolution in time of the average populations on S_1, S_2, and S_3 states. As expected, we observe a fast $S_2 \rightarrow S_1$ electronic relaxation during the first hundreds of femtoseconds of dynamics. The electronic relaxation in [7]CPP is slower compared to that in *m*-alkyl-[7]PPs. Overall, we observe that the greater the bending strain introduced on the conjugated system of *m*-alkyl-[7]PPs (i.e., smaller values of *m*), the slower the electronic energy relaxation process. In the limit of long alkyl tethers, an increase in the S_1 population has rates approaching the limiting values observed in [7]LPP. That is, bent conjugated structures reduce coupling between S_1 and S_2, leading to less efficient $S_2 \rightarrow S_1$ transitions. The dependence of the relaxation rate on the degree of bending strain is more pronounced compared to that previously reported on [*n*]CPPs at room temperature.[26] While internal conversion rates of [*n*]CPPs have shown a significant decrease with the hoop size at low temperature, only a weak dependence persists at 300 K. That is, thermal fluctuations washout differences between effective nonadiabatic couplings on [*n*]CPPs of different sizes. This is not the case for *m*-alkyl-[7]PPs, where significant differences in the internal conversion rates persist even at room temperature. A decreased bending strain between *m*-alkyl-[7]PPs, while elongating the alkyl tether, introduces larger differences in couplings between states than those from insertions of new phenylene units to [*n*]CPPs. This seems to be related to both better structural rigidity and larger gaps, $\Delta E_{1,2}$, between S_1 and S_2 states in bent structures. This is confirmed in Table I, which shows the average over all initial configurations of $\Delta E_{1,2}$ for [7]CPP, *m*-alkyl-[7]PPs (*m* = 1, 4, 7, 10, 13, 16, and 19), and [7]LPP. We observe that $\Delta E_{1,2}$ gradually decreases with the increasing tether length (*m*).

Vibrational relaxation, that takes place concomitantly to electronic relaxation, allows further analysis of the effect of steric hindrance on the internal conversion rates. Figure 6 shows the time evolution of dihedral angles between neighboring phenyls average along the swarm of trajectories. We observe a planarization of the paraphenylene moiety during the energy relaxation process. This behavior has been previously observed, both experimentally and theoretically, during electronic relaxation of other conjugated molecules.[26,47,55−58] During the simulation time, dihedral angles involving the inner phenylenes experience faster torsional reorganizations compared with dihedral angles between

DOI: 10.1021/acs.jpcc.8b05582
J. Phys. Chem. C 2018, 122, 16639−16648

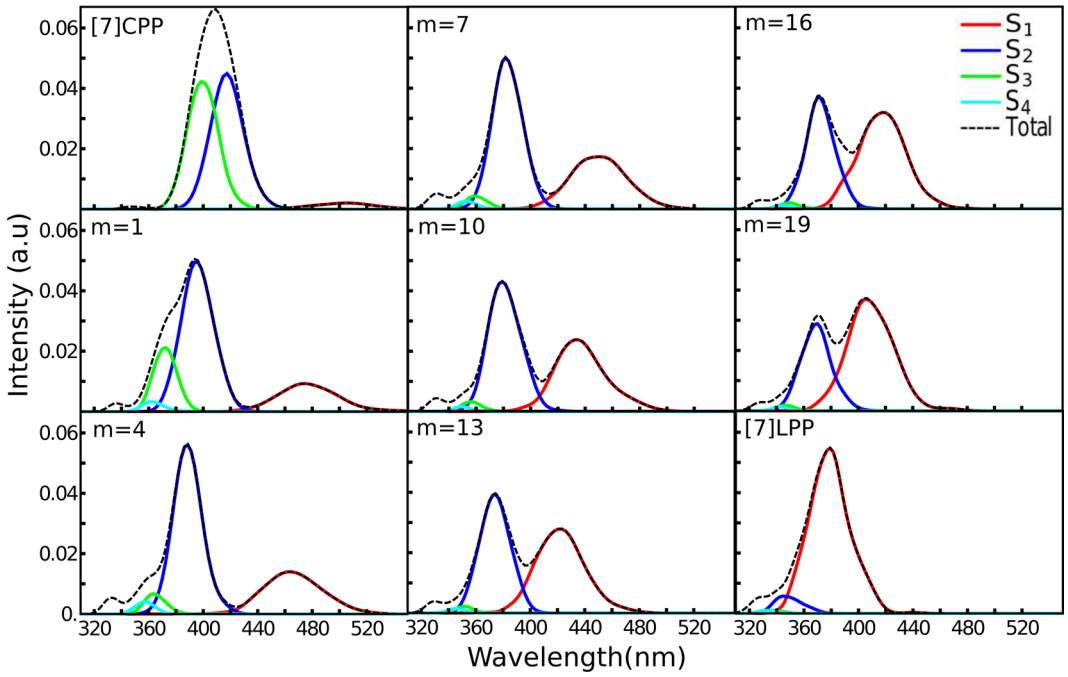

Figure 3. Simulated absorption spectra for [7]CPP, *m*-alkyl-[7]PPs (*m* = 1, 4, 7, 10, 13, 16, and 19), and [7]LPP with separated contributions of different excited states.

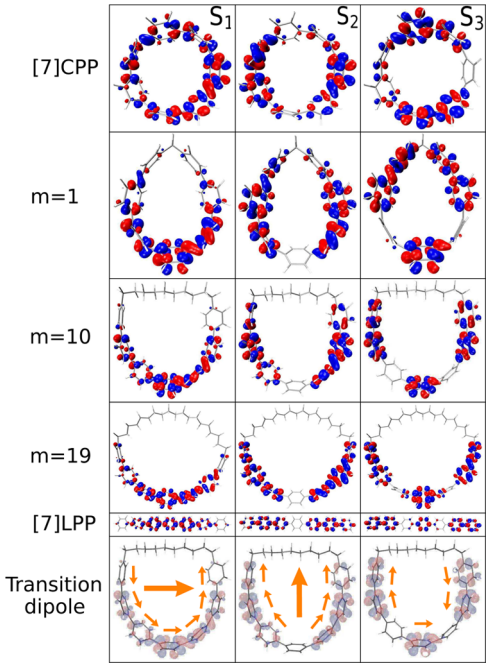

Figure 4. Spatial distribution of transition densities of the essential electronic excited states in [7]CPP, *m*-alkyl-[7]PPs (*m* = 1, 10, and 19), and [7]LPP, calculated at their corresponding ground-state energy minima.

intermediate and outer rings. Differences between initial and final angles, averaged over all *m*, are 5.8, 11.9, and 13.3° for outer, intermediate, and inner torsions, respectively. Comparing these results with the ≈7.0° average difference between dihedral angles in [7]CPP, we can conclude that the introduction of an alkyl tether reduces steric effects that hinder planarization. Nevertheless, outer phenylene units closer to the alkyl tether seem to be subject to additional steric hindrances imposed by the alkyl chain.

As a result of these differential planarization dynamics, the exciton undergoes a directional intramolecular migration from the outer phenylenes to the inner ones. This can be seen in Figure 7 where the time evolution of a fraction of transition density (TD) localized in different rings (eq 4) is depicted. Such outer → inner units intramolecular energy transfer, takes place during the internal conversion process, is clearly seen for all molecules considered. As a result, the exciton becomes spatially localized (self-trapped) on the central portion of the paraphenylene moieties. The spatial exciton extent can be quantified by the participation number, PN(t). For this purpose, we define the fragments as the paraphenylene units. That is, PN(t) varies in the range 1−7. Figure 8 shows the time evolution of PN(t) across ensemble of trajectories for all molecules. The structural disorder introduced by thermal fluctuations prevents PN(t) from reaching maximum possible values close to 7. In fact, PN values corresponding to the ground state equilibrated structures (i.e., initial values of NEXMD simulations) do not exceed 4.6. After photoexcitation, all *m*-alkyl-[7]PPs and [7]LPP demonstrate an exciton self-trapping on less than ∼3.4 rings, that is, close to half of the entire conjugated moiety. This is not the case for [7]CPP, where the exciton size experiences an initial fast reduction and then slowly returns to the nearly original value. Such behavior has been previously reported on [9]CPP in contrast to the observed exciton self-trapping on [*n*]CPPs with larger than 9 values of *n*.[26] According to Figure 7, the localization in *m*-alkyl-[7]PPs occurs at the center of the conjugated segment distant from the alkyl tether, where the rings planarize (Figure 6).

$S_2 \rightarrow S_1$ nonadiabatic transitions involve the activation of nuclear motions in the direction of the nonadiabatic coupling vector.[26,59,60] This electronic coupling between S_2 and S_1 states introduces funneling of electronic energy into a specific

DOI: 10.1021/acs.jpcc.8b05582
J. Phys. Chem. C 2018, 122, 16639−16648

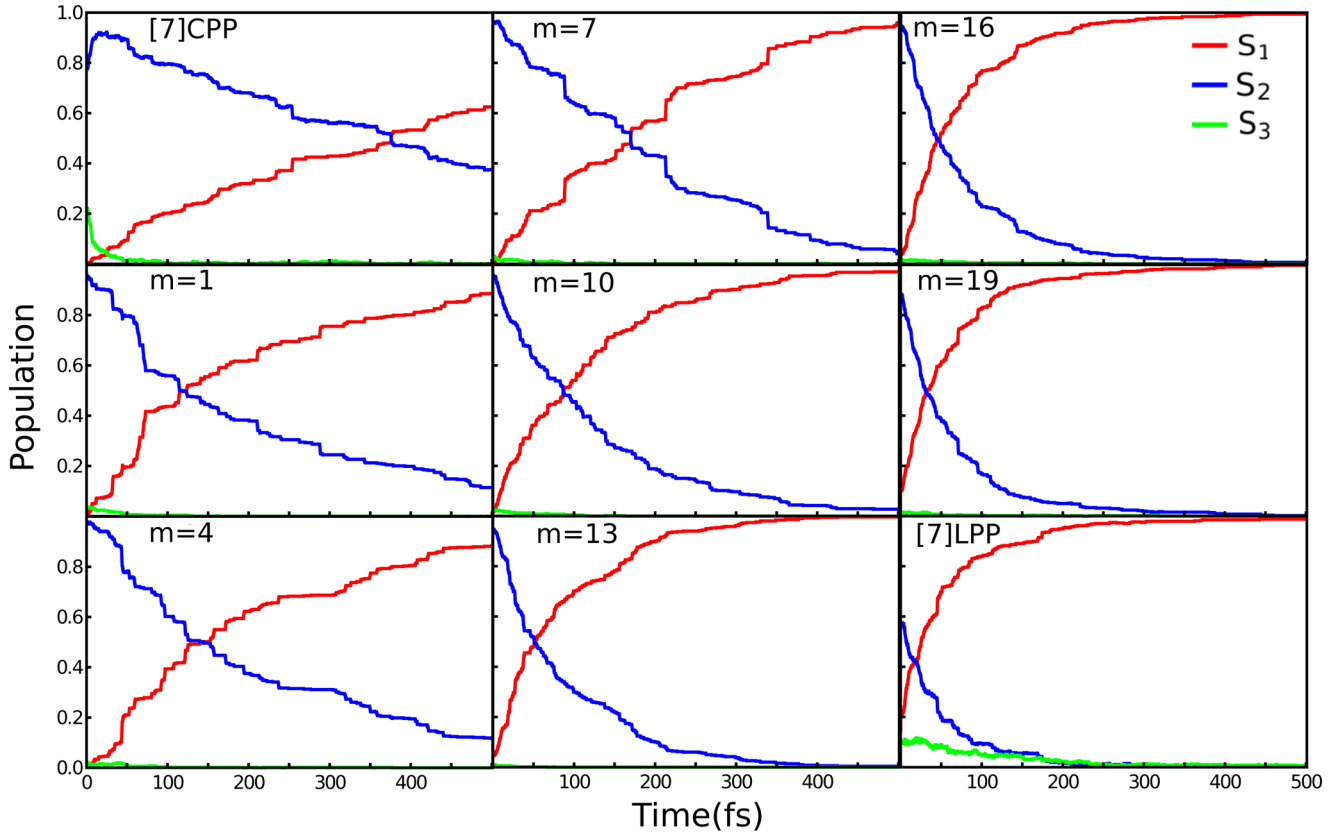

Figure 5. Population of each electronic state as a function of time obtained from the fraction of trajectories in each state for [7]CPP, *m*-alkyl-[7]PPs (*m* = 1, 4, 7, 10, 13, 16, and 19), and [7]LPP.

Table I. Standard Deviation Averaged over All Initial Configurations of the Gap, $\Delta E_{1,2}$, between S_1 and S_2 States

	$\Delta E_{1,2}$ (eV)
[7]CPP	0.502(0.06)
m = 1	0.520(0.09)
m = 4	0.520(0.09)
m = 7	0.478(0.09)
m = 10	0.418(0.10)
m = 13	0.377(0.10)
m = 16	0.359(0.10)
m = 19	0.327(0.09)
[7]LPP	0.267(0.09)

vibrational excitation composed of several normal specific modes. To analyze signatures of such vibronic dynamics, we partition the nanoring into two equivalent halves and further monitor the fraction of TD on each of them. Figure 9 shows the fraction of TD for opposite phenylene units on each half of 4-alkyl-[7]PP as a function of delay time, relative to the moment of hop from S_2 to S_1 states. Subsequent to the nonadiabatic $S_2 \rightarrow S_1$ electronic energy transfer, strictly out-of-phase oscillations in the values of $(\rho_X^{0,S_1}(t))^2$ for each *X* phenylene unit at both sides of the molecule are observed. This behavior is a consequence of the out-of-phase nuclear motion between halves of the paraphenylene moiety induced by electronic transition. These oscillations persist during the first ≈100 fs, after which the molecular system gradually reaches the final equilibration with the bath.

IV. CONCLUSIONS

Bent and curved conjugated molecular systems offer unique optical, structural, and dynamical features that differentiate them from their linear counterparts. In the present work, we have explored transition from a linear oligomer to a circular nanohoop by monitoring gradual changes of these properties in a series of alkyl-tethered-*p*-heptaphenylenes (*m*-alkyl-[7]PPs) by modifying the methylene tether lengths from 1 to 19 carbons.

Here, the tether length controls the bending strain of the paraphenylene moieties. The progressive insertion of new CH_2 units to the alkyl chain systematically reduces steric hindrances, leading to increasing average dihedral angles between the phenyl rings. This behavior resembles the previously reported increase of the average values of dihedral angles with the size of circular nanohoops [*n*]CPPs. Nevertheless, whereas the bending strains are uniformly distributed on [*n*]CPPs, this is not the case for [*m*]-alkyl-[7]PPs.

The gradual increase of the torsions between phenyl units leads to systematic blue shifts of energies of S_1, S_2, and S_3 states contributing to the absorption spectra. This steadily morphs the absorption spectrum of circular system [7]CPP to its linear oligomer limit [7]LPP. The optical selection rules change considerably during this transition. Namely, because of symmetry reasons, the initially optically forbidden S_1 state becomes optically allowed while increasing the length of the alkyl tether. The trend is opposite for the S_3 state undergoing allowed-to-forbidden conversion. Therefore, alkyl-tethered-*p*-phenylenes enable a simple structural mean to tune the desired optical properties, continuously filling the region between the corresponding cyclic and linear conjugated limits.

DOI: 10.1021/acs.jpcc.8b05582
J. Phys. Chem. C 2018, 122, 16639−16648

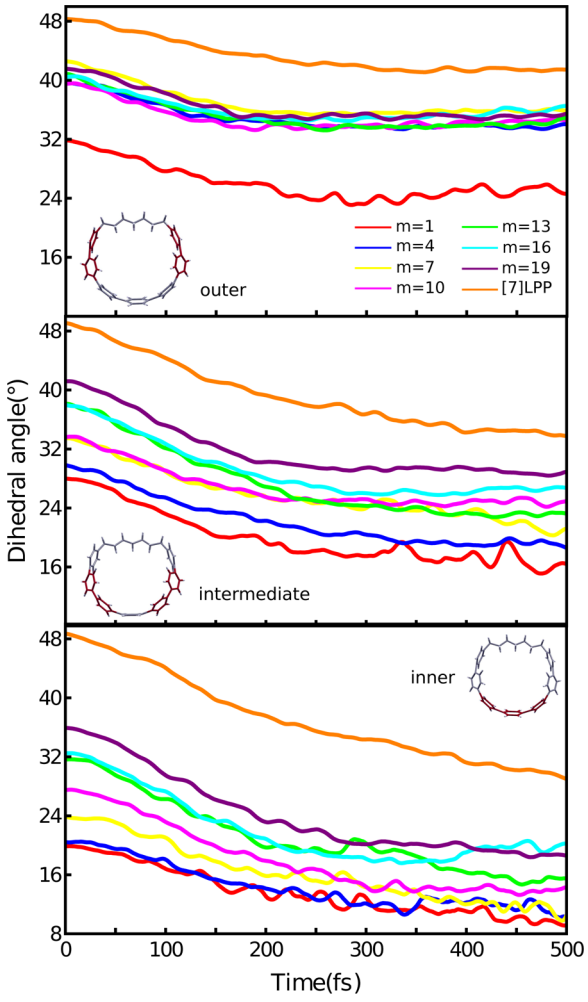

Figure 6. Time evolution of the average dihedral angles between the neighboring phenyls (indicated in red in the schematic representations) for *m*-alkyl-[7]PPs (*m* = 1, 4, 7, 10, 13, 16, and 19) and [7]LPP.

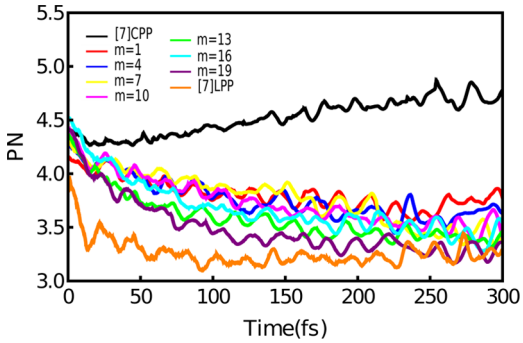

Figure 8. Time evolution of the participation number, PN(t), for [7]CPP, *m*-alkyl-[7]PPs (*m* = 1, 4, 7, 10, 13, 16, and 19), and [7]LPP.

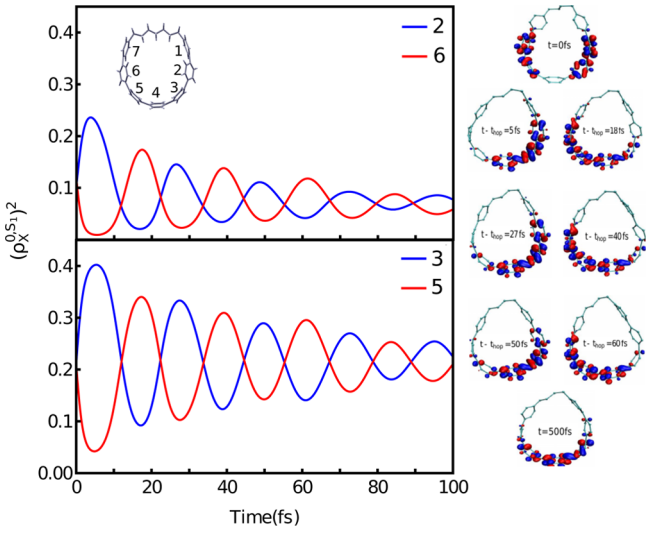

Figure 9. Average fraction of TD for each half of 4-alkyl-[7]PP as a function of delay time, relative to the moment of hop from S_2 to S_1 states. Spatial distribution of transition densities of S_1 at different times is also depicted for a typical NEXMD simulation.

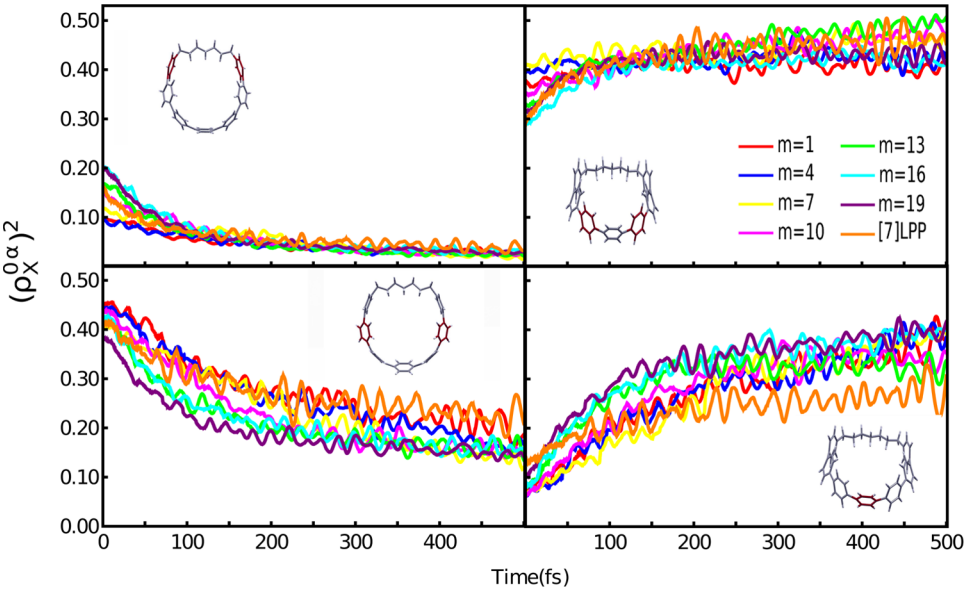

Figure 7. Time evolution of a fraction of TD localized in different phenylene units (indicated in red in the schematic representations) for *m*-alkyl-[7]PPs (*m* = 1, 4, 7, 10, 13, 16, and 19).

DOI: 10.1021/acs.jpcc.8b05582
J. Phys. Chem. C 2018, 122, 16639−16648

NEXMD simulations deliver comprehensive information on the nonradiative electronic and vibrational energy relaxation and redistribution after initial photoexcitation of [7]CPP, *m*-alkyl-[7]PPs (*m* = 1, 4, 7, 10, 13, 16, and 19), and [7]LPP. We observe diminishing electronic energy relaxation rates with an increase of the bending strain introduced in the conjugated system. The slowest and fastest electronic relaxations are attributed to [7]CPP and [7]LPP, respectively, whereas [*m*]-alkyl-[7]PP rates fall in between these limits. Whereas previous studies have shown that thermal fluctuations eliminate differences between nonadiabatic couplings in [*n*]CPPs with different *n*, this is no longer the case in [*m*]-alkyl-[7]PPs systems.

The internal conversion in [7]CPP, [*m*]-alkyl-[7]PPs, and [7]LPP leads to a planarization of the paraphenylene moiety. This process is not uniform across the dihedral angles of [*m*]-alkyl-[7]PPs. Namely, the central phenyl units undergo the most significant torsional reorganization. As a consequence of these differential planarizations, the exciton experiences a directional intramolecular migration toward the center of the conjugated system. This behavior is contrasting to the random exciton localization previously observed in [*n*]CPPs.

Finally, the nonadiabatic $S_2 \rightarrow S_1$ electronic transition in [*m*]-alkyl-[7]PPs facilitates efficient excitation of transient out-of-phase nuclear motion between halves of the conjugated segment that ultimately promotes periodic oscillatory evolution of the excitonic wave function on the lower state. This behavior evidences the close relationship between excitonic dynamical localization and delocalization patterns accompanying transfer of electronic energy into vibrations during the internal conversion process.

■ ASSOCIATED CONTENT

Supporting Information

The Supporting Information is available free of charge on the ACS Publications website at DOI: 10.1021/acs.jpcc.8b05582.

Spatial distribution of transition densities of the S_4 electronic excited state in [7]CPP, *m*-alkyl-[7]PPs (*m* = 1, 10, and 19), and [7]LPP, calculated at their corresponding ground-state energy minima (Figure S1) (PDF)

Simulated absorption spectra, evaluated using geometries obtained at the end of our NEXMD simulations for [7]CPP, *m*-alkyl-[7]PPs (*m* = 1, 4, 7, 10, 13, 16, and 19), and [7]LPP with separated contributions of different excited states (Figure S2) (PDF)

m = $4_1$00, $10_1$00, and $16_1$00 fs correspond to spatial distribution of electronic transition density for 4-alkyl-[7]PP, 10-alkyl-[7]PP, and 16-alkyl-[7]PP as a function of delay time, relative to the moment of hop from S_2 to S_1 states; spatial distribution of transition densities of S_1 at different times (Movies S1−S3) (MPG)(MPG)-(MPG)

■ AUTHOR INFORMATION

Corresponding Author

*E-mail: sfalberti@gmail.com. Tel: +54-11-436-57100-5659.

ORCID

S. Tretiak: 0000-0001-5547-3647

S. Fernández-Alberti: 0000-0002-0916-5069

Notes

The authors declare no competing financial interest.

■ ACKNOWLEDGMENTS

B.R.-H., D.O.-A, and S.F.-A. are supported by CONICET, UNQ, ANPCyT (PICT- 2014-2662). S.T. acknowledges support from Los Alamos National Laboratory (LANL) Directed Research and Development Funds. LANL is operated by Los Alamos National Security, LLC, for the National Nuclear Security Administration of the U.S. Department of Energy under contract DE-AC52-06NA25396. This work was performed in part at the Center for Integrated Nanotechnology (CINT), a U.S. Department of Energy, Office of Basic Energy Sciences user facility. We also acknowledge the LANL Institutional Computing (IC) Program for providing computational resources.

■ REFERENCES

(1) Li, C.; Liu, M.; Pschirer, N. G.; Baumgarten, M.; Müllen, K. Polyphenylene-Based Materials for Organic Photovoltaics. *Chem. Rev.* **2010**, *110*, 6817−6855.

(2) Facchetti, A. π-Conjugated Polymers for Organic Electronics and Photovoltaic Cell Applications. *Chem. Mater.* **2011**, *23*, 733−758.

(3) Guo, X.; Baumgarten, M.; Müllen, K. Designing π-Conjugated Polymers for Organic Electronics. *Prog. Polym. Sci.* **2013**, *38*, 1832−1908.

(4) Nelson, T.; Fernandez-Alberti, S.; Roitberg, A. E.; Tretiak, S. Electronic Delocalization, Vibrational Dynamics and Energy Transfer in Organic Chromophores. *J. Phys. Chem. Lett.* **2017**, *8*, 3020−3031.

(5) Iyoda, M.; Yamakawa, J.; Rahman, M. Conjugated Macrocycles: Concepts and Applications. *Angew. Chem., Int. Ed.* **2011**, *50*, 10522−10553.

(6) Hu, L.; Guo, Y.; Yan, X.; Zeng, H.; Zhou, J. Electronic Transport Properties in [n]Cycloparaphenylenes Molecular Devices. *Phys. Lett. A* **2017**, *381*, 2107−2111.

(7) Lewis, S. E. Cycloparaphenylenes and Related Nanohoops. *Chem. Soc. Rev* **2015**, *44*, 2221−2304.

(8) Golder, M. R.; Jasti, R. Syntheses of the Smallest Carbon Nanohoops and the Emergence of Unique Physical Phenomena. *Acc. Chem. Res.* **2015**, *48*, 557−566.

(9) Segawa, Y.; Fukazawa, A.; Matsuura, S.; Omachi, H.; Yamaguchi, S.; Irle, S.; Itami, K. Combined Experimental and Theoretical Studies on the Photophysical properties of cycloparaphenylenes. *Org. Biomol. Chem.* **2012**, *10*, 5979−5984.

(10) Kawase, T.; Kurata, H. Ball-, Bowl-, and Belt-Shaped Conjugated Systems and Their Complexing Abilities: Exploration of the Concave-Convex π-π Interaction. *Chem. Rev.* **2006**, *106*, 5250−5273.

(11) Steinberg, B. D.; Scott, L. T. New Strategies for Synthesizing Short Sections of Carbon Nanotubes. *Angew. Chem., Int. Ed.* **2009**, *48*, 5400−5402.

(12) Bodwell, G. J. Growth potential. *Nat. Nanotechnol.* **2010**, *5*, 103−104.

(13) Jasti, R.; Bertozzi, C. Progress and Challenges for the Bottom-up Synthesis of Carbon Nanotubes with Discrete Chirality. *Chem. Phys. Lett.* **2010**, *494*, 1−7.

(14) Van Raden, J. M.; Louie, S.; Zakharov, L. N.; Jasti, R. 2,2′-Bipyridyl-embedded Cycloparaphenylenes as a General Strategy to Investigate Nanohoop-based Coordination Complexes. *J. Am. Chem. Soc.* **2017**, *139*, 2936−2939.

(15) Wong, B. M. Optoelectronic Properties of Carbon Nanorings: Excitonic Effects from Time-Dependent Density Functional Theory. *J. Phys. Chem. C* **2009**, *113*, 21921−21927.

(16) Peña-Alvarez, M.; Qiu, L.; Taravillo, M.; Baonza, V.; Ruiz-Delgado, M.; Yamago, S.; Jasti, R.; López-Navarrete, J.; Casado, J.; Kertesz, M. From Linear to Cyclic Oligoparaphenylenes: Electronic and Molecular Changes Traced in the Vibrational Raman Spectra and Reformulation of the Bond Length Alternation Pattern. *Phys. Chem. Chem. Phys.* **2016**, *18*, 11683−11692.

DOI: 10.1021/acs.jpcc.8b05582
J. Phys. Chem. C 2018, 122, 16639−16648

(17) Darzi, E. R.; Jasti, R. The Dynamic, Size-Dependent Properties of [5]-[12]Cycloparaphenylenes. *Chem. Soc. Rev.* **2015**, *44*, 6401−6410.
(18) Segawa, Y.; Omachi, H.; Itami, K. Theoretical Studies on the Structures and Strain Energies of Cycloparaphenylenes. *Org. Lett.* **2010**, *12*, 2262−2265.
(19) Nishihara, T.; Segawa, Y.; Itami, K.; Kanemitsu, Y. Excited States in Cycloparaphenylenes: Dependence of Optical Properties on Ring Length. *J. Phys. Chem. Lett.* **2012**, *3*, 3125−3128.
(20) Nishihara, T.; Segawa, Y.; Itami, K.; Kanemitsu, Y. Exciton Recombination Dynamics in Nanoring Cycloparaphenylenes. *Chem. Sci.* **2014**, *5*, 2293−2296.
(21) Kim, P.; Park, K. H.; Kim, W.; Tamachi, T.; Iyoda, M.; Kim, D. Relationship between Dynamic Planarization Processes and Exciton Delocalization in Cyclic Oligothiophenes. *J. Phys. Chem. Lett.* **2015**, *6*, 451−456.
(22) Adamska, L.; Nayyar, I.; Chen, H.; Swan, A. K.; Oldani, N.; Fernandez-Alberti, S.; Golder, M. R.; Jasti, R.; Doorn, S. K.; Tretiak, S. Self-Trapping of Excitons, Violation of Condon Approximation, and Efficient Fluorescence in Conjugated Cycloparaphenylenes. *Nano Lett.* **2014**, *14*, 6539−6546.
(23) Li, P.; Sisto, T.; Darzi, E. R.; Jasti, R. The Effects of Cyclic Conjugation and Bending on the Optoelectronic Properties of Paraphenylenes. *Org. Lett.* **2014**, *16*, 182−185.
(24) Nelson, T.; Fernandez-Alberti, S.; Roitberg, A. E.; Tretiak, S. Nonadiabatic Excited-State Molecular Dynamics: Modeling Photophysics in Organic Conjugated Materials. *Acc. Chem. Res.* **2014**, *47*, 1155−1164.
(25) Nelson, T.; Fernandez-Alberti, S.; Chernyak, V.; Roitberg, A.; Tretiak, S. Nonadiabatic Excited-State Molecular Dynamics Modeling of Photoinduced Dynamics in Conjugated Molecules. *J. Phys. Chem. B* **2011**, *115*, 5402−5414.
(26) Oldani, N.; Doorn, S. K.; Tretiak, S.; Fernandez-Alberti, S. Photoinduced Dynamics in Cycloparaphenylenes: Planarization, Electron-Phonon Coupling, Localization and Intra-Ring Migration of the Electronic Excitation. *Phys. Chem. Chem. Phys.* **2017**, *19*, 30914−30924.
(27) Nelson, T.; Fernandez-Alberti, S.; Chernyak, V.; Roitberg, A. E.; Tretiak, S. Nonadiabatic Excited-State Molecular Dynamics: Numerical Tests of Convergence and Parameters. *J. Chem. Phys.* **2012**, *136*, No. 054108.
(28) Tully, J. C. Molecular Dynamics with Electronic Transitions. *J. Chem. Phys.* **1990**, *93*, 1061−1071.
(29) Hammes-Schiffer, S.; Tully, J. C. Proton Transfer in Solution: Molecular Dynamics with Quantum Transitions. *J. Chem. Phys.* **1994**, *101*, 4657−4667.
(30) Tretiak, S.; Mukamel, S. Density Matrix Analysis and Simulation of Electronic Excitations in Conjugated and Aggregated Molecule. *Chem. Rev.* **2002**, *102*, 3171−3212.
(31) Chernyak, V.; Schulz, M. F.; Mukamel, S.; et al. Krylov-Space Algorithms for Time-Dependent Hartree-Fock and Density Functional Computations. *J. Chem. Phys.* **2000**, *113*, 36−43.
(32) Tretiak, S.; Isborn, C. M.; Niklasson, A. M. N.; Challacombe, M. Representation Independent Algorithms for Molecular Response Calculations in Time-Dependent Self-Consistent Field Theories. *J. Chem. Phys.* **2009**, *130*, No. 054111.
(33) Tretiak, S.; Chernyak, V. Resonant Nonlinear Polarizabilities in the Time-Dependent Density Functional Theory. *J. Chem. Phys.* **2003**, *119*, 8809−8823.
(34) Furche, F.; Ahlrichs, R. Adiabatic Time-Dependent Density Functional Methods for Excited State properties. *J. Chem. Phys.* **2002**, *117*, 7433−7447.
(35) Tommasini, M.; Chernyak, V.; Mukamel, S. Electronic Density-Matrix Algorithm for Nonadiabatic Couplings in Molecular Dynamics Simulations. *Int. J. Quantum Chem.* **2001**, *85*, 225−238.
(36) Send, R.; Furche, F. First-Order Nonadiabatic Couplings from Time-Dependent Hybrid Density Functional Response Theory: Consistent Formalism, Implementation, and Performance. *J. Chem. Phys.* **2010**, *132*, No. 044107.
(37) van Gunsteren, W. F.; Berendsen, H. J. C. Algorithms for Brownian Dynamics. *Mol. Phys.* **1982**, *45*, 637−647.
(38) Tretiak, S.; Chernyak, V.; Mukamel, S. Two-Dimensional Real-Space Analysis of Optical Excitations in Acceptor-Substituted Carotenoids. *J. Am. Chem. Soc.* **1997**, *119*, 11408−11419.
(39) Tretiak, S.; Chernyak, V.; Mukamel, S. Collective Electronic Oscillators for Nonlinear Optical Response of Conjugated Molecules. *Chem. Phys. Lett.* **1996**, *259*, 55−61.
(40) Dewar, M. J. S.; Zoebisch, E. G.; Healy, E. F.; Stewart, J. J. P. AM1: A New General Purpose Quantum Mechanical Molecular Model. *J. Am. Chem. Soc.* **1985**, *107*, 3902−3909.
(41) Thouless, D. J. *The Quantum Mechanics of Many-Body Systems*; Academic Press, 1972.
(42) Davidson, E. R. *Reduced Density Matrices in Quantum Chemistry*; Academic Press, 1976.
(43) Bazan, G. C.; Oldham, W. J., Jr.; Lachicotte, R. J.; Tretiak, S.; Chernyak, V.; Mukamel, S. Stilbenoid Dimers: Dissection of a Paracyclophane Chromophore. *J. Am. Chem. Soc.* **1998**, *120*, 9188−9204.
(44) Tretiak, S.; Chernyak, V.; Mukamel, S. A Excited Electronic States of Carotenoids: Time-Dependent Density-Matrix-Response Algorithm. *J. Quantum Chem.* **1998**, *70*, 11−727.
(45) Abe, A., Dusek, K., Kobayashi, S., Eds.; *Emissive Materials − Nanomaterials*; Advances in Polymer Science; Springer-Verlag: Berlin, Heidelberg, 2006; Vol. *199*, p 292.
(46) Oldani, N.; Tretiak, S.; Bazan, G.; Fernandez-Alberti, S. Modeling of Internal Conversion in Photoexcited Conjugated Molecular Donor used in Organic Photovoltaics. *Energy Environ. Sci.* **2014**, *7*, 1175−1184.
(47) Ondarse-Alvarez, D.; Oldani, N.; Tretiak, S.; Fernandez-Alberti, S. Computational Study of Photoexcited Dynamics in Bichromophoric Cross-Shaped Oligofluorene. *J. Chem. Phys. A* **2014**, *118*, 10742−10753.
(48) Fernandez-Alberti, S.; Roitberg, A. E.; Nelson, T.; Tretiak, S. Identification of Unavoided Crossings in Nonadiabatic Photoexcited Dynamics Involving Multiple Electronic States in Polyatomic Conjugated Molecules. *J. Chem. Phys.* **2012**, *137*, No. 014512.
(49) Nelson, T.; Fernandez-Alberti, S.; Roitberg, A. E.; Tretiak, S. Nonadiabatic Excited-State Molecular Dynamics: Treatment of Electronic Decoherence. *J. Chem. Phys.* **2013**, *138*, No. 224111.
(50) Wu, C.; Malinin, S. V.; Tretiak, S.; Chernyak, V. Exciton Scattering and Localization in Branched Dendrimeric Structures. *Nat. Phys.* **2006**, *2*, 631−635.
(51) Mewes, S. A.; Mewes, J. M.; Dreuw, A.; Plasser, F. Excitons in Poly(para phenylene vinylene): A Quantum-Chemical Perspective Based on High-Level ab Initio Calculations. *Phys. Chem. Chem. Phys.* **2016**, *18*, 2548−2563.
(52) Magyar, R. J.; Tretiak, S.; Gao, Y.; Wang, H. L.; Shreve, A. P. A Joint Theoretical and Experimental Study of Phenylene-Acetylene Molecular Wires. *Chem. Phys. Lett.* **2005**, *401*, 149−156.
(53) Jasti, R.; Bhattacharjee, J.; Neaton, J. B.; Bertozzi, C. R. Synthesis, Characterization, and Theory of [9]-, [12]-, and [18]-Cycloparaphenylene: Carbon Nanohoop Structures. *J. Am. Chem. Soc.* **2008**, *130*, 17646−17647.
(54) Sundholm, D.; Tauberta, S.; Pichierrib, F. Calculation of Absorption and Emission Spectra of [n]Cycloparaphenylenes: the Reason for the Large Stokes Shift. *Phys. Chem. Chem. Phys.* **2010**, *12*, 2751−2757.
(55) Clark, J.; Nelson, T.; Tretiak, S.; Cirmi, G.; Lanzani, G. Femtosecond Torsional Relaxation. Conformational Dynamics of Photoexcited Conjugated Molecules. *Nat. Phys.* **2012**, *8*, 225−231.
(56) Tretiak, S.; Saxena, A.; Martin, R. L.; Bishop, A. R. Conformational Dynamics of Photoexcited Conjugated Molecules. *Phys. Rev. Lett.* **2002**, *89*, No. 097402.
(57) Karabunarliev, S.; Baumgarten, M.; Bittner, E. R.; Müllen, K. Rigorous Franck-Condon Absorption and Emission Epectra of Conjugated Oligomers from Quantum Chemistry. *J. Chem. Phys.* **2000**, *113*, 11372−11381.

DOI: 10.1021/acs.jpcc.8b05582
J. Phys. Chem. C 2018, 122, 16639−16648

(58) Franco, I.; Tretiak, S. Electron-Vibrational Dynamics of Photoexcited Polyfluorenes. *J. Am. Chem. Soc.* **2004**, *126*, 12130−12140.
(59) Soler, M. A.; Roitberg, A. E.; Nelson, T.; Tretiak, S.; Fernandez-Alberti, S. Analysis of State-Specific Vibrations Coupled to the Unidirectional Energy Transfer in Conjugated Dendrimers. *J. Phys. Chem. A* **2012**, *116*, 9802−9810.
(60) Soler, M. A.; Roitberg, A. E.; Nelson, T.; Tretiak, S.; Fernandez-Alberti, S. Signature of Nonadiabatic Coupling in Excited-State Vibrational Modes. *J. Phys. Chem. A* **2014**, *118*, 10372−10379.

DOI: 10.1021/acs.jpcc.8b05582
J. Phys. Chem. C 2018, 122, 16639−16648